Title
Adsorption and desorption of cationic malachite green dye on cellulose nanofibril aerogels

Authors
Jiang, Feng
Dinh, Darren M
Hsieh, You-Lo

Publication Date
2017-10-01

DOI
10.1016/j.carbpol.2017.05.097

Peer reviewed

Carbohydrate Polymers 173 (2017) 286–294

Contents lists available at ScienceDirect

Carbohydrate Polymers

journal homepage: www.elsevier.com/locate/carbpol

Adsorption and desorption of cationic malachite green dye on cellulose nanofibril aerogels

Feng Jiang, Darren M. Dinh, You-Lo Hsieh*

Fiber and Polymer Science, University of California, Davis, CA 95616, USA

ARTICLE INFO

Article history:
Received 14 March 2017
Received in revised form 5 May 2017
Accepted 31 May 2017
Available online 4 June 2017

Keywords:
Aerogel
Cellulose nanofibrils
Cationic dye
Malachite green
Adsorption
Desorption

ABSTRACT

Ultra-light aerogels have been assembled from cellulose nanofibrils into hierarchically macroporous (several hundred μm) honeycomb cellular structure surrounded with mesoporous (8–60 nm) thin walls. The high specific surface (193 m^2/g) and surface carboxyl content (1.29 mmol/g) of these aerogels were demonstrated to be highly capable of removing cationic malachite green (MG) dye from aqueous media. The rapid MG adsorption was driven by electrostatic interactions and followed a pseudo-second-order adsorption kinetic and monolayer Langmuir adsorption isotherm. At a low 1:5 mg/mL aerogel/MG ratio, both initial MG adsorption rate (2.3–59.8 mg g^{-1} min^{-1}) and equilibrium adsorption capacity (53.0–203.7 mg g^{-1}) increased with increasing initial MG concentrations from 10 to 200 mg/L, reaching a maximum adsorption of 212.7 mg g^{-1}. The excellent dye removal efficiency was demonstrated by complete MG removal through four repetitive adsorptions at a low 1:5 mg/mL aerogel/MG ratio and 10 mg/L dye concentration as well as 92% MG adsorption in a single batch at one order of magnitude higher10:5 mg/mL aerogel/MG ratio and 100 mg/L dye concentration. The adsorbed MG in aerogels could be desorbed in aqueous media by increasing ionic strength, demonstrating facile recovery of both dye and aerogel as well as the robust capability of this aerogel for repetitive applications.

1. Introduction

Most consumer products, such as textile, paper, leather, food and cosmetic goods, are colored using synthetic dyes that, along with other auxiliary chemicals, produce vast discharges to pose allergic, carcinogenic, mutagenic and toxic threats to aquatic life and humans (Chowdhury, Mishra, Saha, & Kushwaha, 2011; Namasivayam, Muniasamy, Gayatri, Rani, & Ranganathan, 1996). Organic dye molecules also have strong tendency to chelate metal ions to increase toxicity to fish and other organisms. Furthermore, dyes in water bodies absorb light to impede light penetration and reduce photosynthetic activities and inhibit growth of aquatic plants (Garg, Amita, Kumar, & Gupta, 2004; Salleh, Mahmoud, Karim, & Idris, 2011). Dyes in the wastewater streams can be removed by adsorption, sedimentation, filtration, chemical coagulation, oxidation or treated with microorganisms, etc. (Gupta & Suhas, 2009). Among these methods, adsorption is most common due to its low cost, simplicity and ease of operation (Garg, Kumar, & Gupta, 2004).

Malachite green (MG), a *N*-methylated diaminotriarylmethane cationic dye, has been widely used as a parasiticide, fungicide and antiprotozoan in aquaculture (Srivastava, Sinha, & Roy, 2004), medical disinfectant and anthelmintic (Culp & Beland, 1996). When left untreated, MG could enter into the food chains from accumulation in living organisms as cytotoxic, mutagenic, teratological and carcinogenic threats to mammalian cells (Fernandes, Lalitha, & Rao, 1991; Rao, 1995). MG has been removed from aqueous system via adsorption using clay (Arellano-Cardenas, Lopez-Cortez, Cornejo-Mazon, & Carlos Mares-Gutierrez, 2013), carbonaceous (Ghaedi, Hajati, Zare, & Jaberi, 2015; Hameed & El-Khaiary, 2008a; Hammud, Shmait, & Hourani, 2015; Liu, Zhou, Shen, Liu, & Zhang, 2015; Malik, Ramteke, & Wate, 2007; Mall, Srivastava, Agarwal, & Mishra, 2005; Wang, Liu, Jiang, Yu, & Chen, 2015; Zhang et al., 2015) and magnetic absorbents (Sun et al., 2015), chitin and chitosan (Bekci, Oezveri, Seki, & Yurdakoc, 2008; Tang, Zhou, & Zhang, 2012), alga (Bekci, Seki, & Cavas, 2009), and lignocellulosic biomass (Chowdhury & Das Saha, 2013; Chowdhury et al., 2011; Garg, Kumar et al., 2004; Gong, Jin, Chen, Chen, & Liu, 2006; Hameed & El-Khaiary, 2008b; Khattri & Singh, 2009; Zhou et al., 2015). Modified agricultural residues, such as NaOH treated rice husks and ground rice bran, only showed low MG adsorption capacities of less than 20 mg/g (Chowdhury et al., 2011) and 50 mg/g (Wang, Zhou, Jiang, & Sun, 2008), respectively. As cellulose nanofibrils (CNFs)

* Corresponding author.
E-mail address: ylhsieh@ucdavis.edu (Y.-L. Hsieh).

http://dx.doi.org/10.1016/j.carbpol.2017.05.097
0144-8617/

derived from 2,2,6,6-tetramethylpyperidine-1-oxyl (TEMPO) oxidization contain surface carboxylate groups, they are expected to adsorb cationic dyes. However, TEMPO CNFs from poplar could only adsorb 3.7 mg/g cationic methylene blue, not much higher than the 2.9 mg/g adsorption capacity of the uncharged CNFs isolated by ultrasonication from the same source (Chen et al., 2014). This low adsorption capacity could not be reconciled as the surface charge nature of TEMPO oxidized CNFs was not reported. On the other hand, mechanically defibrillated kenaf core CNFs with surface adsorbed anionic lignin and hemicellulose did improve methylene blue adsorption capacity to 122 mg/g (Chan, Chia, Zakaria, Sajab, & Chin, 2015), indicating the benefit of anionic charge to cationic dye adsorption. Therefore, cationic dye adsorption on TEMPO oxidized CNFs towards cationic dyes remain to be elucidated, especially in light of their surface charge characteristics.

In this study, anionically charged CNFs were derived at 97% yield from rice straw cellulose via coupled TEMPO mediated oxidation and blending to carry 1.29 mmol/g surface carboxyls, among which 86% in the sodium carboxylate form (Jiang, Han, & Hsieh, 2013; Jiang & Hsieh, 2013). These highly negatively charged CNFs were self-assembled into hydrogels via freezing (−20 °C, 12 h)-thawing (ambient temperature) then freeze-dried into superlight and superabsorbent aerogels that exhibited excellent wet resiliency for easy handling and recovery in aqueous media (Jiang & Hsieh, 2014b; Jiang & Hsieh, 2014c). To further increase the specific surface, inter-CNF hydrogen bondings were reduced by solvent exchange the hydrogels with *tert*-butanol prior to freeze-drying into aerogels. The adsorption mechanism, kinetics and capacity of cationic malachite green dyes on these cellulose nanofibril aerogels as well as their desorption were investigated.

2. Materials and methods

2.1. Materials

Pure cellulose was isolated from rice straw (Calrose variety) following a previously reported process to a 36% yield (Lu & Hsieh, 2012). Cellulose nanofibrils (CNFs) were derived from pure rice straw cellulose employing 5 mmol NaClO per gram of cellulose and mechanical blending at 37,000 rpm for 30 min (Jiang et al., 2013). Malachite green (Fisher Scientific), sodium chloride (NaCl, >99%, Fisher Scientific), and *tert*-butanol (certified, Fisher Scientific) were used as received without further purification. All water used was purified and deionized by Milli-Q plus water purification system (Millipore Corporate, Billerica, MA).

2.2. Cellulose aerogel preparation

Aqueous CNF suspension (10 mL, 0.5 wt%) in a conical shaped centrifuge glass tube (14 mm inner diameter) was frozen at −20 °C for 5 h and thawed at ambient temperature into CNF hydrogels that were solvent exchanged sequentially in 25%, 50%, 75% and 100% *tert*-butanol. The alcohol gels were then solvent-exchanged in 100% *tert*-butanol three more times to remove water completely, then lyophilized at −50 °C in a freeze-drier (FreeZone 1.0L Benchtop Freeze Dry System, Labconco, Kansas City, MO) for 2 days to yield CNF aerogels.

2.3. Cellulose aerogel characterization

CNF aerogel was cut in the transverse direction, coated with gold and visualized by a field emission scanning electron microscope (FE-SEM) (XL 30-SFEG, FEI/Philips, USA) at a 5-mm working distance and 5-kV accelerating voltage. The specific surface and pore characteristics of CNF aerogel were determined by N_2 adsorption at 77 K by a surface area and porosity analyzer (ASAP 2000, Micromeritics, USA). The specific surface was determined by the Brunauer-Emmett-Teller (BET) method from linear region of the isotherms in the 0.06–0.20 relative P/P_0 pressure range. Pore size distributions were derived from desorption branch of the isotherms by the Barrett–Joyner–Halenda (BJH) method. The total pore volumes were estimated from the amount adsorbed at a relative pressure of $P/P_0 = 0.98$. CNF aerogels before and after dye adsorption (MG concentration of 100 mg/L, dried in air) were pressed into KBr pellets (1:100, w/w). The FTIR spectra were collected from a Thermo Nicolet 6700 spectrometer at ambient conditions in the transmittance mode from an accumulation of 128 scans at a 4 cm^{-1} resolution over the regions of 4000–400 cm^{-1}.

2.4. Adsorption of malachite green

Adsorption study was carried out by immersing 10 mg aerogel absorbent in 50 mL of malachite green absorbent solution (1:5 mg/mL aerogel to MG solution w/v ratio) at MG concentrations ranging from 10 to 400 mg/L under constant magnetic stirring at ambient temperature for 2 h. It should be noted that the self assembled CNFs are super-resilient in aqueous media as reported before (Jiang & Hsieh, 2014b; Jiang & Hsieh, 2014c) and do not change shape during dye adsorption or desorption. At fixed time intervals, the concentration of dye solution was measured at 617 nm using UV–vis spectrophotometer (Evolution 600, Thermo Scientific). The amount of malachite green adsorbed at each time interval on the aerogel was calculated as:

$$q_e = \frac{(c_0 - c_e) \times V}{m} \quad (1)$$

where q_e is the amount of dye adsorbed, c_0 is the initial dye concentration and c_e is the equilibrium dye concentration, V is the solution volume and m is the mass of aerogel.

The percentage of MG removal was calculated as:

$$Percentage\ of\ removal = \frac{(c_0 - c_e)}{c_0} \times 100\% \quad (2)$$

MG adsorption was also carried out at 1:5–10:5 aerogel to MG solution ratios with 100 mg/L MG concentration.

For MG removal from dilute solution, the adsorption was carried out at 10 mg/L MG concentration and 1:5 aerogel-to-MG v/w ratio for 2 h. After adsorption, a piece of fresh aerogel was put into the residual solution for three repeated times until the solution becomes colorless.

2.5. Desorption of malachite green

Desorption of MG was investigated on CNF aerogels with pre-adsorbed dye (158 mg g^{-1}, 100 mg/L MG, 1:5 w/v aerogel-to-MG solution ratio for 2 h) in 50 mL of 0, 50 and 200 mM sodium chloride solutions. At fixed time intervals, the concentration of salt solution was measured at 617 nm using UV–vis spectrophotometer, and the experiment stopped once there were negligible changes in absorbance for 3 consecutive readings. The percentage of dye desorption was calculated as:

$$Dye\ desorption = \frac{c_e \times V}{m \times q_e} \times 100\% \quad (3)$$

where c_e is the equilibrium dye concentration, V is the volume of NaCl solution, m is the mass of the aerogel, and q_e is the equilibrium dye amount on the aerogel after 2 h adsorption in 100 mg/L MG solution.

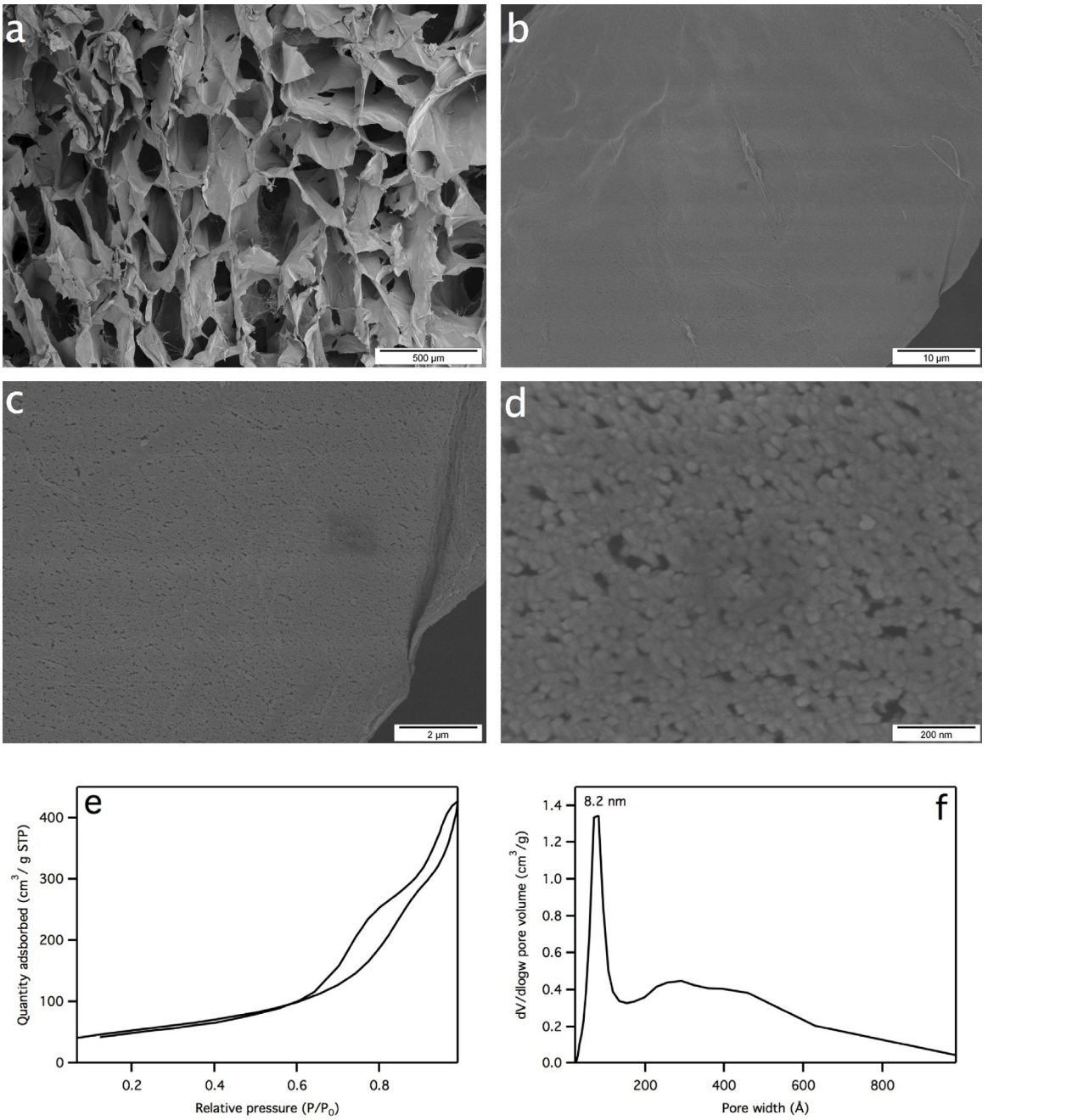

Fig. 1. SEM images of CNF aerogel with progressively increased magnification, showing honey comb porous structure (a), as well as mesoporous structure on the cell walls (b–d). BET N_2 adsorption-desorption isotherm (e) and pore size distribution (f) of CNF aerogel.

3. Results and discussion

3.1. Characterization of CNF aerogel

Cellulose nanofibrils (CNFs) were isolated from rice straw cellulose via TEMPO oxidation followed by mechanical blending to be 1–2 nm wide and 500–1000 nm long, carrying 1.29 mmol/g surface carboxyl groups (Jiang et al., 2013). Aqueous CNFs (0.5 wt%) suspension was frozen (−20 °C) and thawed (ambient temperature) into hydrogel, then solvent exchanged with *tert*-butanol to alcohol gel that was freeze-dried into aerogel (Jiang & Hsieh, 2014b). The CNF aerogel had a honeycomb-like cellular structure that consisted of a few hundred micrometers wide irregularly shaped cells or spaces surrounded by thin walls of self-assembled CNFs (Fig. 1a). Closer examination of the thin cell walls showed numerous 50 nm or smaller mesopores (Fig. 1b–d). The hundreds of microns wide honeycomb cells were shaped by large ice crystals slowly grown at −20 °C, concentrating CNFs around ice crystals to self-assemble into thin films driven by both hydrogen bonding and van der Waals interactions, whereas the mespores were spacings created from steric hindrance of CNF surface bound *tert*-butanol that inhibit CNF association. This effect is similar to *tert*-butanol exchanging aqueous CNF suspensions at concentrations one magnitude lower, i.e., up to 0.05%, to reduce self-assembling of CNFs into much narrower tens of nanometer wide fibers instead of sub-micron wide fibers (Jiang & Hsieh, 2014a).

CNF aerogel showed type IV nitrogen adsorption-desorption hysteresis isotherm (Fig. 1e), typical for mesoporous material with 193.1 m^2/g specific surface and 0.65 cm^3/g total pore volume, 16 and 32 times of those without *tert*-butanol exchange

($12\ m^2/g$ and $0.02\ cm^3/g$), respectively (Jiang & Hsieh, 2014b; Jiang & Hsieh, 2014c). The mesopore widths peaked at 8.2 nm and ranged broadly up to 60 nm (Fig. 1f), consistent with the numerous mesopores observed by high resolution SEM (Fig. 1d). These highly mesoporous thin walls explain the significantly increased specific surface whereas the hierarchical macroporous honeycomb cell structures could facilitate mass transportation of liquid.

3.2. Adsorption kinetics

The adsorption of MG dye onto CNF aerogels (1:5 mg/mL aerogel/MG w/v ratio) occurred rapidly during the first 40 min, then leveling off beyond 80 min at all initial MG concentrations from 10 to 400 mg/L (Fig. 2a). The MG adsorption rate increased with the increasing initial dye concentrations and is consistent with the higher concentration gradient. The total MG adsorbed increased from 44 to 206 mg/g at 10–400 mg/L original concentrations, with 76–99% of which was adsorbed during the first 40 min (Fig. 2b). This fast adsorption capacity is attributed to the hierarchical macro- and mesoporous structure of the aerogels. The percentage of MG removed from aqueous dye solutions, however, decreased with increasing initial concentrations, i.e., from 75 to 78% at the lower 10–25 mg/L to 20 and 10% at the higher 200 and 400 mg/L concentrations, respectively (Fig. 2c).

The adsorption kinetics of MG on CNF aerogel were evaluated with both Lagergren's pseudo-first-order and Ho's pseudo-second-order models. The Lagergren's pseudo-first-order model was expressed as (Lagergren, 1898):

$$q_t = q_e \times (1 - e^{-k_1 \times t}) \tag{4}$$

and fitted with a nonlinear regression program (Kaleidagraph, version 4.5.2, Synergy Software). The Ho's pseudo-second-order model was expressed as (Ho & McKay, 1999):

$$q_t = \frac{q_e^2 \times k_2 \times t}{1 + q_e \times k_2 \times t} \tag{5}$$

where q_t and q_e are the amount of MG adsorbed at time t and equilibrium (mg/g), k_1 is the pseudo-first-order rate constant (min^{-1}) and k_2 is the pseudo-second-order rate constant ($g\,mg^{-1}\,min^{-1}$). Eq. (5) could be linearized as:

$$\frac{t}{q_t} = \frac{1}{k_2 \times q_e^2} + \frac{1}{q_e} \times t \tag{6}$$

The adsorption data were plotted as t/q_t versus t and fitted to linear expression with Igor Pro 6.22A (WaveMetrics Inc.), giving linear plot as shown in Fig. 2d. The initial adsorption rate v_0 at $t = 0$ could be calculated from Eq. (6):

$$v_0 = k_2 \times q_e^2 \tag{7}$$

While both kinetic models of the adsorption data yielded correlation coefficient R^2 values over 0.97 (Table 1), pseudo-second order kinetic model was clearly a better fit with all R^2 values above 0.9943, showing linearity in the t/q_t versus t plots (Fig. 2d). This indicates that the overall rate of the MG adsorption onto CNF aerogels is controlled by chemisorption. From pseudo-second order kinetic model, MG dye adsorption capacity (q_e) increased from 53.0 to 203.7 $mg\,g^{-1}$ and initial MG adsorption rate (v_0) increased from 2.25 to 59.8 $mg\,g^{-1}\,min^{-1}$, respectively, with increasing original dye concentrations from 10 to 200 mg/L.

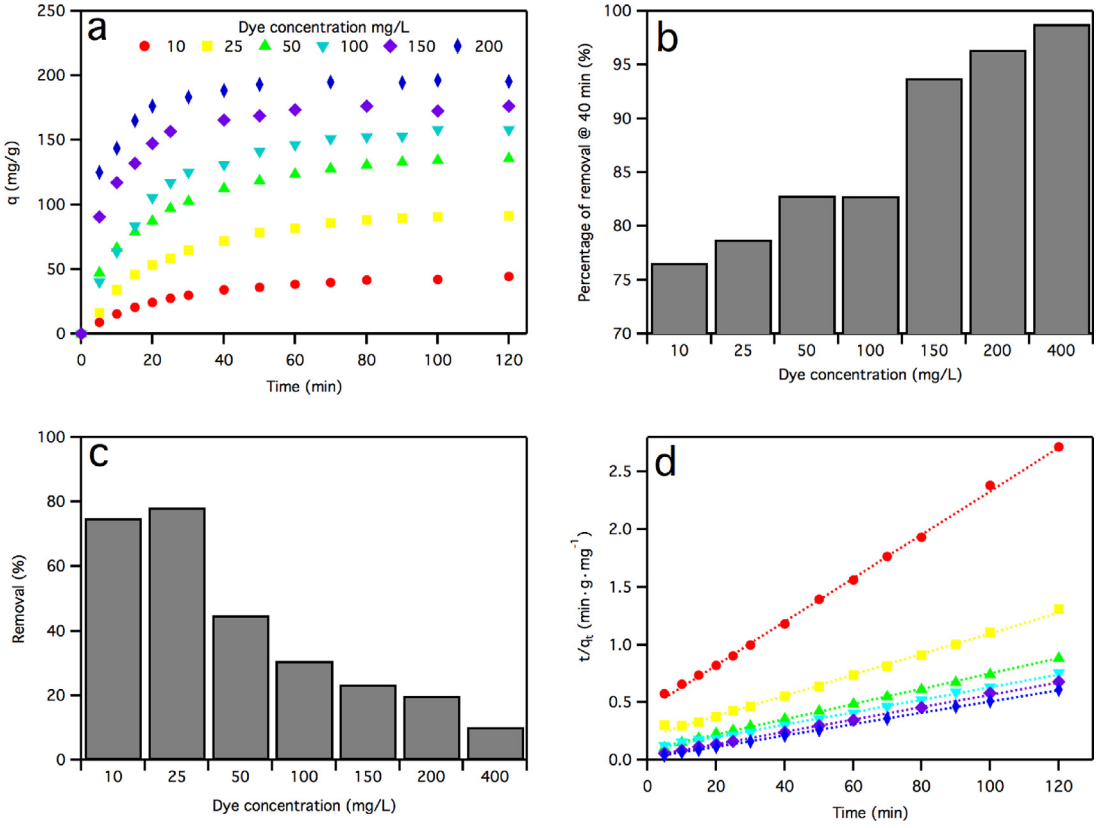

Fig. 2. Adsorption of malachite green (10–400 mg/L) onto CNF aerogel with 1:5 mg/mL aerogel-MG w/v ratios (a), percentage of removal of the maximum adsorbed dye at 40 min (b), percentage of removal of the total dye content (c), and pseudo-second-order adsorption kinetics (d).

Table 1
Pseudo-first and pseudo-second order kinetic model parameters for MG adsorption onto CNF aerogels.

C_0 (mg/L)	Pseudo-first-order			Pseudo-second-order			
	q_e (mg g^{-1})	k_1 (min^{-1})	R^2	q_e (mg g^{-1})	k_2(g mg^{-1} min^{-1})	v_0(mg g^{-1} min^{-1})	R^2
10	42.7	0.041	0.9964	53.0	0.80×10^{-3}	2.25	0.9964
25	90.6	0.043	0.9972	111.5	0.40×10^{-3}	3.73	0.9975
50	130.2	0.059	0.9786	151.2	0.49×10^{-3}	11.2	0.9969
100	155.0	0.054	0.9965	184.4	0.33×10^{-3}	11.2	0.9943
150	171.0	0.12	0.9843	186.9	0.96×10^{-3}	33.5	0.9970
200	190.9	0.16	0.9801	203.7	1.44×10^{-3}	59.8	0.9963

3.3. Adsorption mechanism

The adsorption mechanism of dyes in the solution into an absorbent generally follows three steps, i.e., bulk diffusion of dye molecules in the solution to the boundary layer on the adsorbent surfaces, film diffusion of dye molecules from the boundary layer into the adsorbent surface and intra-particle diffusion of dye molecules from the adsorbent surface into the adsorbent interior (Crini, Peindy, Gimbert, & Robert, 2007; Hameed & El-Khaiary, 2008a). As the slowest intra-particle diffusion being usually the rate-determining step, the Weber's intra-particle diffusion model was applied (Weber & Morris, 1963):

$$q_t = k_i \times t^{\frac{1}{2}} + C \tag{8}$$

where q_t is the MG quantity adsorbed at time t, k_i is the intra-particle diffusion rate constant (mg g^{-1} $min^{-1/2}$), and C is a constant that represents the thickness or resistance of the boundary layer. The q_t versus $t_{1/2}$ should be linear and pass through the origin if the intra-particle diffusion is the only controlling step.

The intra-particle diffusion plots of q_t versus $t_{1/2}$ at all dye concentrations showed three linear regions that do not pass through the origin (Fig. 3a), suggesting MG adsorption onto CNF aerogel to be controlled by more than one mechanism. The initial steeper slope is thought to be due to the accelerated film diffusion through the boundary layer enhanced by the strong electrostatic interaction between the aerogel surface carboxylate groups and the MG iminium cations. The more moderate second stage is attributed to the intra-particle diffusion of MG into the aerogel interior and is also the rate-controlling step, whereas the final nearly leveled regions signal reaching the equilibrium.

The intra-particle diffusion rate constant k_i and boundary layer thickness or resistance constant C values were calculated from the second intra-particle diffusion region using Eq. (8) to yield R^2 ranging from 0.9835 to 0.9961, very high at all concentrations (Fig. 3b). The k_i values increased with increasing dye concentrations at up to 100 mg/L, then decreased, the latter may be attributed to the charge repulsion between MG at higher concentrations, similar to the report on the high resistance of MG diffusion on rattan sawdust (Hameed & El-Khaiary, 2008b) and cyclodextrin-based adsorbent (Crini et al., 2007). The boundary layer thickness constant C also increased with increasing MG concentrations, indicating greater adsorption via the initial electrostatic interaction at higher MG concentrations.

3.4. Adsorption isotherm

To further understand how MG is adsorbed onto CNF aerogels as well as to determine the equilibrium data, the adsorbed quantities and residual dyes in the solution were fitted in both Langmuir and Freundlich isotherms. The Langmuir adsorption isotherm represents monolayer adsorption onto a finite number of homogeneous sites and is described as (Langmuir, 1918):

$$q_e = \frac{q_{max} \times K_L \times C_e}{1 + K_L \times C_e} \tag{9}$$

where q_e is the adsorbed MG at equilibrium (mg/g), q_{max} is the adsorption capacity (mg/g), K_L is the equilibrium adsorption constant (L/mg), and C_e is the equilibrium MG concentration in the solution.

Freundlich adsorption isotherm describes adsorption of adsorbates onto a heterogeneous surfaces with different functional groups or adsorbent-adsorbate interactions and is expressed as (Freundlich, 1907):

$$q_e = K_F \times C_e^{1/n} \tag{10}$$

where K_F is the Freundlich constant ((mg/g)(L/g)^n) and n is the heterogeneity factor.

Linear relationships of Langmuir and Freundlich isotherms could be expressed as Eqs. (11) and (12), respectively:

$$\frac{C_e}{q_e} = \frac{C_e}{q_{max}} + \frac{1}{K_L \times q_{max}} \tag{11}$$

a

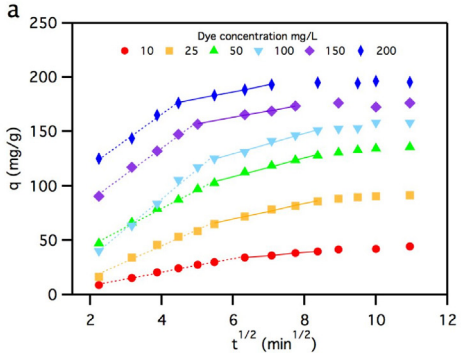

b

C_0 (mg/L)	k_i (mg·g^{-1}·min$^{-1/2}$)	C (mg/g)	R^2
10	2.92	15.4	0.9874
25	7.16	26.4	0.9881
50	8.59	56.9	0.9835
100	9.38	73.3	0.9876
150	6.02	126.9	0.9963
200	6.44	147.9	0.9991

Fig. 3. Intra-particle diffusion model plot for MG adsorption onto CNF aerogels at 1:5 mg/mL aerogel/dye w/v ratios with 10–200 mg/L dye concentration (a); Intra-particle diffusion model constant and correlation coefficient for MG adsorption onto CNF aerogels at 1:5 mg/mL aerogel/dye w/v ratios with 10–400 mg/L dye concentration (b).

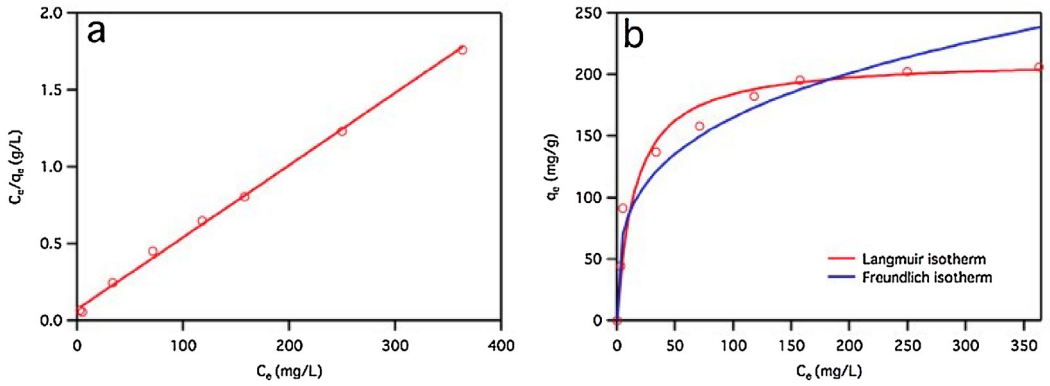

c

Sample	Langmuir isotherm			Freundlich isotherm		
	q_m (mg/g)	b_L (L/mg)	R^2	k_F (L/g)	nF (mg/g)(L/g)^n	R^2
CNF aerogel	212.7	0.065	0.9980	44.7	0.284	0.8930

Fig. 4. Langmuir adsorption isotherm fitting (a), and experimental data with both Langmuir and Freundlich isotherm fitting (b), adsorption isotherm parameter for the adsorption of malachite green by CNF aerogel at 1:5 mg/mL aerogel/dye w/v ratios with 10–400 mg/L dye concentration (c).

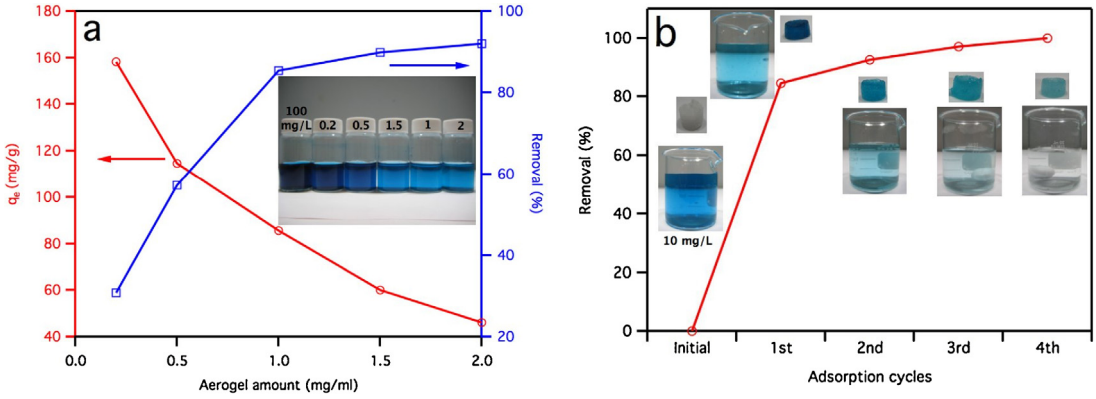

Fig. 5. Effectiveness of MG removal by CNF aerogels: (a) aerogel dosage (1:5–10:5 mg/mL aerogel/dye w/v rations) on MG (100 mg/L) adsorption and removal at 2 h, inset are pictures of the original dye solutions; (b) complete removal of malachite green (10 mg/L) with 1:5 mg/mL aerogel/MG w/v ratio by cyclic adsorption, insets are pictures of dye solutions and aerogels.

$$lnq_e = lnK_F + \frac{1}{n} \times lnC_e \quad (12)$$

The Langmuir plot of Ce/qe versus Ce showed a linear regression curve with slope of $1/q_{max}$ and intercept of $1/(K_L{*}q_{max})$ (Fig. 4a) as well as a high R^2 of 0.9980 (Fig. 4c), indicating good linear fitting. In contrast, the Freundlich isotherm (Fig. 4b) had a much lower R^2 of 0.8930, showing a poorer fit. Therefore, well-fit Langmuir isotherm indicates MG adsorbed as a monolayer on CNF aerogel surfaces at a maximum adsorption quantity of 212.7 mg g^{-1}.

3.5. Effectiveness of CNF aerogel in complete removal of malachite green

The effectiveness of CNF aerogel to remove MG dye was first evaluated using varying aerogel quantities at a constant 100 mg/L MG concentration. Removal of MG increased from 30.8 to 92.0% with increasing aerogel/MG ratios from 1:5 to 10:5 mg/mL (Fig. 5a). The equilibrium MG adsorbed in CNF aerogels decreased from 158.3 to 46.0 mg g^{-1} with increasing aerogel/MG ratios. MG removal at a dilute 10 mg/L MG concentration was further detailed by repetitive adsorption using fresh aerogels of the least quantity, i.e., 1:5 mg/mL aerogel/MG ratio (Fig. 5b). Removal of MG increased from 84.5% to 92.6, 97.0 and 99.9% in the 2nd, 3rd, and 4th adsorption cycles, respectively, leaving colorless solution after the 4th. Therefore, repetitive adsorption using fresh aerogels is effective in completely removing MG at low concentrations.

3.6. MG-CNF aerogel interactions

TEMPO oxidized CNFs contain 1.29 mmol/g surface carboxyls, of which 86% is in sodium carboxylate form as confirmed from FTIR peak at 1618 cm^{-1} and a small shoulder at 1720 cm^{-1} (Fig. 6a), corresponding to carbonyl stretching of sodium carboxylate and carboxylic acid groups (Fig. 6b), respectively. As sodium carboxylate dissociates, the negatively charged carboxylate anions on CNF surfaces can electrostatically attract the MG iminium cations (Fig. 6c). The FTIR spectra of MG adsorbed CNF aerogel showed several peaks in the 800–400 cm^{-1} fingerprint region, consistent of the mono-substituted and para-disubstituted benzene rings in MG and confirming its presence in the aerogel. This was further supported by the sharp peak at 1585 cm^{-1} assigned for the C=C stretching of the benzene ring, as well as the peak at 1376 cm^{-1} due to $-CH_3$

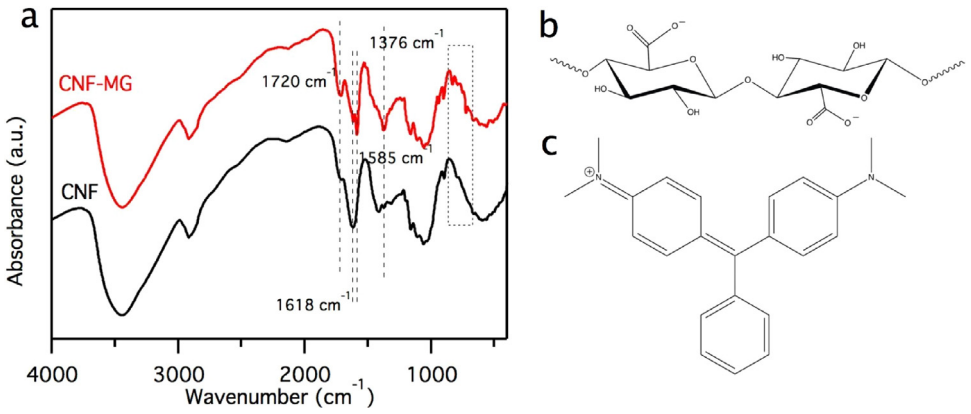

Fig. 6. (a) FTIR spectra of CNF aerogel before and after malachite green adsorption; chemical structures of (b) TEMPO oxidized cellulose chains on the CNF surface and (c) malachite green.

stretching in malachite green. The sodium carboxylate carbonyl peak at 1618 cm^{-1} became smaller which could be due to the interaction between the carboxylate and iminium groups, whereas the carboxylic acid peak at 1720 cm^{-1} remained essentially unchanged, suggesting that the carboxylic acid did not participate in the adsorption. Therefore, FTIR spectra further confirmed electrostatic interactions to be predominantly responsible for MG dye adsorption onto CNF aerogel. The maximum adsorption of 212.7 mg g^{-1} MG/aerogel corresponds to 0.59 mmol/g MG/aerogel or approximately 46% of the CNF surface carboxyls were involved in binding MG. Considering 14% of surface carboxyls being carboxylic acid that did not dissociate into charged species, the 40% remaining carboxyls may be inaccessible due to steric hindrance and/or charge repulsion of the adsorbed MG, as well as being buried within the aerogel that can not be approached by MG.

3.7. Desorption of malachite green from CNF aerogel

Upon immersion in deionized water for 1 h, only 16% MG preadsorbed in CNF aerogel (158 mg g^{-1}, 100 mg/L MG, 1:5 mg/mL aerogel/MG w/v ratio, 2 h) was desorbed (Fig. 7a), showing most MG to be strongly bond to the CNF aerogel. With added NaCl at 50 and 200 mM concentrations, significantly higher 65 and 85% of adsorbed MG were released within 1 h. Such enhanced desorption was clearly evident by the lighter aerogel colors in the presence of NaCl and at the higher concentration. The enhanced dye desorption with increasing ionic strength is consistent with the electrostatic interaction mechanism of MG adsorption on aerogel. In solutions of high ionic strength, the negative charged CNFs and positive charged MG would be screened by the respective Na^+ and Cl^- counter ions, breaking their electrostatic bonds and releasing MG molecules.

MG dye desorption from aerogels at varied NaCl concentrations also fitted to pseudo-second order kinetic well, with all R^2 above

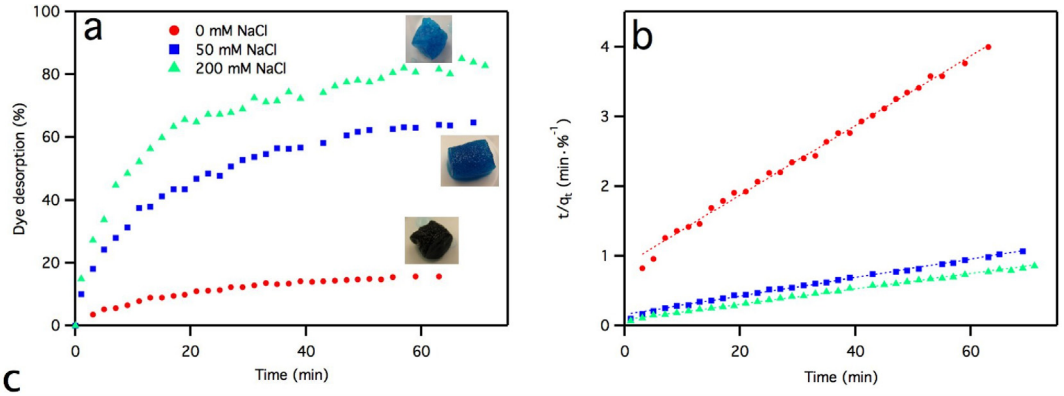

c

NaCl (C_0)	Pseudo-second-order			
	q_e (%)	K_2 (%$^{-1}$·min^{-1})	V_0 (%/min)	R^2
0 mM	20.1	2.83×10-3	1.14	0.9972
50 mM	75.6	1.08×10-3	6.15	0.9961
200 mM	90.5	1.41×10-3	11.6	0.9958

Fig. 7. Desorption of malachite green from CNF aerogel at varied salt concentrations, insets are pictures of aerogels after desorption (a); fitting of pseudo-second-order desorption kinetics (b); Pseudo second order kinetics fitting parameters for dye desorption from CNF aerogels (c).

0.9958 (Fig. 7b & c). The initial desorption rate increased from 1.14 to 6.15 and 11.56% min^{-1} with increasing NaCl concentrations from 0 to 50 and 200 mM, respectively, recovering 90.5% adsorbed MG at 200 mM NaCl at equilibrium. The remaining less than 10% of residual dyes could be removed using a fresh NaCl solution. The substantial and fast desorption process indicates that the aerogel could be facilely regenerated for repeated dye removal applications.

4. Conclusions

Ultra-lightweight aerogels have been fabricated from TEMPO oxidized cellulose nanofibrils (CNFs) via a three-step freezing-thawing induced hydrogel formation, *tert*-butanol exchange and freeze-drying to a honeycomb cellular structure consisting of a few hundred μm wide irregularly shaped open cells surrounded by mesoporous (8–60 nm) thin walls of self-assembled CNFs. This unique hierarchical macro- and meso-porous structure coupled with high specific surface (193 m^2/g) and surface carboxyl (1.29 mmol/g) has shown to be highly effective in removing cationic dye via electrostatic interactions between the CNF surface anionic carboxylate groups and MG iminium groups. At a low 1:5 mg/mL aerogel/MG ratio, dye adsorption increased with time, adsorbing 76–99% of dye in 10–400 mg/L MG concentrations in 40 min. With increasing initial dye concentrations from 10 to 200 mg/L, the adsorption kinetics of MG on CNF aerogels showed a pseudo-second-order adsorption model with the initial adsorption rate increasing from 2.3 to 59.8 mg g^{-1} min^{-1} and the equilibrium adsorption capacity increasing from 53.0 to 203.7 mg g^{-1} The MG adsorption on CNF aerogels exhibited a monolayer Langmuir adsorption isotherm with maximum adsorption of 212.7 mg g^{-1}, corresponding to participation of 46% of the total surface carboxyls. The CNF aerogel showed over 92% MG removal efficiency in a single batch adsorption at 10:5 mg/mL aerogel/MG w/v ratio and 100 mg/L dye concentration. Complete MG dye removal was possible at a low 1:5 mg/mL aerogel/MG w/v ratio and a low 10 mg/L dye concentration in four repetitive adsorptions. Over 90% of adsorbed dye could be released in 200 mM NaCl solution at an initial desorption rate of 11.6% min^{-1}. The excellent wet resiliency and fast release of the adsorbed dye could be achieved by increasing ionic strength to recover the aerogel for repetitive use.

Funding

The authors appreciate the funding support by the California Rice Research Board (Project RU-9) and the AgTech Innovation Center at University of California, Davis.

References

Arellano-Cardenas, S., Lopez-Cortez, S., Cornejo-Mazon, M., & Carlos Mares-Gutierrez, J. (2013). Study of malachite green adsorption by organically modified clay using a batch method. *Applied Surface Science*, *280*, 74–78.
Bekci, Z., Oezveri, C., Seki, Y., & Yurdakoc, K. (2008). Sorption of malachite green on chitosan bead. *Journal of Hazardous Materials*, *154*(1–3), 254–261.
Bekci, Z., Seki, Y., & Cavas, L. (2009). Removal of malachite green by using an invasive marine alga Caulerpa racemosa var. cylindracea. *Journal of Hazardous Materials*, *161*(2–3), 1454–1460.
Chan, C. H., Chia, C. H., Zakaria, S., Sajab, M. S., & Chin, S. X. (2015). Cellulose nanofibrils: A rapid adsorbent for the removal of methylene blue. *RSC Advances*, *5*(24), 18204–18212.
Chen, W., Li, Q., Wang, Y., Yi, X., Zeng, J., Yu, H., et al. (2014). Comparative study of aerogels obtained from differently prepared nanocellulose fibers. *ChemSusChem*, *7*(1), 154–161.
Chowdhury, S., & Das Saha, P. (2013). Adsorption of malachite green from aqueous solution by naoh-modified rice husk: Fixed-bed column studies. *Environmental Progress & Sustainable Energy*, *32*(3), 633–639.
Chowdhury, S., Mishra, R., Saha, P., & Kushwaha, P. (2011). Adsorption thermodynamics, kinetics and isosteric heat of adsorption of malachite green onto chemically modified rice husk. *Desalination*, *265*(1–3), 159–168.
Crini, G., Peindy, H. N., Gimbert, F., & Robert, C. (2007). Removal of CI Basic Green 4 (Malachite Green) from aqueous solutions by adsorption using cyclodextrin-based adsorbent: Kinetic and equilibrium studies. *Separation and Purification Technology*, *53*(1), 97–110.
Culp, S. J., & Beland, F. A. (1996). Malachite green: A toxicological review. *Journal of the American College of Toxicology*, *15*(3), 219–238.
Fernandes, C., Lalitha, V. S., & Rao, K. V. K. (1991). Enhancing effect of malachite green on the development of hepatic preneoplastic lesions induced by n-nitrosodiethylamine in rats. *Carcinogenesis*, *12*(5), 839–845.
Freundlich, H. (1907). *Z. Phyzik. Chem.*, *57*, 385.
Garg, V. K., Amita, M., Kumar, R., & Gupta, R. (2004). Basic dye (methylene blue) removal from simulated wastewater by adsorption sawdust: A timber using Indian Rosewood industry waste. *Dyes and Pigments*, *63*(3), 243–250.
Garg, V. K., Kumar, R., & Gupta, R. (2004). Removal of malachite green dye from aqueous solution by adsorption using agro-industry waste: A case study of Prosopis cineraria. *Dyes and Pigments*, *62*(1), 1–10.
Ghaedi, M., Hajati, S., Zare, M., & Jaberi, S. Y. S. (2015). Experimental design for simultaneous analysis of malachite green and methylene blue; derivative spectrophotometry and principal component-artificial neural network. *RSC Advances*, *5*(49), 38939–38947.
Gong, R., Jin, Y., Chen, F., Chen, J., & Liu, Z. (2006). Enhanced malachite green removal from aqueous solution by citric acid modified rice straw. *Journal of Hazardous Materials*, *137*(2), 865–870.
Gupta, V. K., & Suhas. (2009). Application of low-cost adsorbents for dye removal – A review. *Journal of Environmental Management*, *90*(8), 2313–2342.
Hameed, B. H., & El-Khaiary, M. I. (2008a). Kinetics and equilibrium studies of malachite green adsorption on rice straw-derived char. *Journal of Hazardous Materials*, *153*(1–2), 701–708.
Hameed, B. H., & El-Khaiary, M. I. (2008b). Malachite green adsorption by rattan sawdust: Isotherm, kinetic and mechanism modeling. *Journal of Hazardous Materials*, *159*(2–3), 574–579.
Hammud, H. H., Shmait, A., & Hourani, N. (2015). Removal of Malachite Green from water using hydrothermally carbonized pine needles. *RSC Advances*, *5*(11), 7909–7920.
Ho, Y. S., & McKay, G. (1999). Pseudo-second order model for sorption processes. *Process Biochemistry*, *34*(5), 451–465.
Jiang, F., & Hsieh, Y.-L. (2013). Chemically and mechanically isolated nanocellulose and their self-assembled structures. *Carbohydrate Polymers*, *95*(1), 32–40.
Jiang, F., & Hsieh, Y.-L. (2014a). Assembling and redispersibility of rice straw nanocellulose: Effect of tert-butanol. *ACS Applied Materials & Interfaces*, *6*(22), 20075–20084.
Jiang, F., & Hsieh, Y.-L. (2014b). Super water absorbing and shape memory nanocellulose aerogels from TEMPO-oxidized cellulose nanofibrils via cyclic freezing-thawing. *Journal of Materials Chemistry A*, *2*(2), 350–359.
Jiang, F., & Hsieh, Y. L. (2014). Amphiphilic superabsorbent cellulose nanofibril aerogels. *Journal of Materials Chemistry A*, *2*(18), 6337–6342.
Jiang, F., Han, S., & Hsieh, Y.-L. (2013). Controlled defibrillation of rice straw cellulose and self-assembly of cellulose nanofibrils into highly crystalline fibrous materials. *RSC Advances*, *3*(30), 12366–12375.
Khattri, S. D., & Singh, M. K. (2009). Removal of malachite green from dye wastewater using neem sawdust by adsorption. *Journal of Hazardous Materials*, *167*(1–3), 1089–1094.
Lagergren, S. (1898). Zur theorie der sogenannten adsorption geloster stoffeKungliga Svenska Vetenskapsakademiens. *Handlingar*, *24*(4), 1–39.
Langmuir, I. (1918). The adsorption of gases on plane surfaces of glass, mica and platinum. *Journal of the American Chemical Society*, *40*(9), 42.
Liu, A., Zhou, W., Shen, K., Liu, J., & Zhang, X. (2015). One-pot hydrothermal synthesis of hematite-reduced graphene oxide composites for efficient removal of malachite green from aqueous solution. *RSC Advances*, *5*(22), 17336–17342.
Lu, P., & Hsieh, Y. L. (2012). Preparation and characterization of cellulose nanocrystals from rice straw. *Carbohydrate Polymers*, *87*(1), 564–573.
Malik, R., Ramteke, D. S., & Wate, S. R. (2007). Adsorption of malachite green on groundnut shell waste based powdered activated carbon. *Waste Management*, *27*(9), 1129–1138.
Mall, I. D., Srivastava, V. C., Agarwal, N. K., & Mishra, I. M. (2005). Adsorptive removal of malachite green dye from aqueous solution by bagasse fly ash and activated carbon-kinetic study and equilibrium isotherm analyses. *Colloids and Surfaces A–Physicochemical and Engineering Aspects*, *264*(1–3), 17–28.
Namasivayam, C., Muniasamy, N., Gayatri, K., Rani, M., & Ranganathan, K. (1996). Removal of dyes from aqueous solutions by cellulosic waste orange peel. *Bioresource Technology*, *57*(1), 37–43.
Rao, K. V. K. (1995). Inhibition of DNA synthesis in primary rat hepatocyte cultures by malachite green: A new liver tumor promoter. *Toxicology Letters*, *81*(2–3), 107–113.
Salleh, M. A. M., Mahmoud, D. K., Karim, W. A. W. A., & Idris, A. (2011). Cationic and anionic dye adsorption by agricultural solid wastes: A comprehensive review. *Desalination*, *280*(1–3), 1–13.
Srivastava, S., Sinha, R., & Roy, D. (2004). Toxicological effects of malachite green. *Aquatic Toxicology*, *66*(3), 319–329.
Sun, L., Hu, S., Sun, H., Guo, H., Zhu, H., Liu, M., et al. (2015). Malachite green adsorption onto Fe3O4@SiO2-NH2: Isotherms, kinetic and process optimization. *RSC Advances*, *5*(16), 11837–11844.
Tang, H., Zhou, W., & Zhang, L. (2012). Adsorption isotherms and kinetics studies of malachite green on chitin hydrogels. *Journal of Hazardous Materials*, *209*, 218–225.

Wang, X. S., Zhou, Y., Jiang, Y., & Sun, C. (2008). The removal of basic dyes from aqueous solutions using agricultural by-products. *Journal of Hazardous Materials*, *157*(2–3), 374–385.

Wang, D., Liu, L., Jiang, X., Yu, J., & Chen, X. (2015). Adsorption and removal of malachite green from aqueous solution using magnetic beta-cyclodextrin-graphene oxide nanocomposites as adsorbents. *Colloids and Surfaces A–Physicochemical and Engineering Aspects*, *466*, 166–173.

Weber, W. J. J., & Morris, J. C. (1963). Kinetics of adsorption on carbon from solution. *Journal of the Sanitary Engineering Division by American Society of Civil Engineers*, *89*, 31–59.

Zhang, X., Yu, H., Yang, H., Wan, Y., Hu, H., Zhai, Z., et al. (2015). Graphene oxide caged in cellulose microbeads for removal of malachite green dye from aqueous solution. *Journal of Colloid and Interface Science*, *437*, 277–282.

Zhou, Y., Min, Y., Qiao, H., Huang, Q., Wang, E., & Ma, T. (2015). Improved removal of malachite green from aqueous solution using chemically modified cellulose by anhydride. *International Journal of Biological Macromolecules*, *74*, 271–277.